Purified meta-Cresol Purple dye perturbation: how it influences spectrophotometric pH measurements

Xinyu Li [a], Maribel I. García-Ibáñez [a,+], Brendan R. Carter [b,c], Baoshan Chen [a], Qian Li [a], Regina A. Easley [d], Wei-Jun Cai [a]*

a. School of Marine Science and Policy, University of Delaware, Newark, DE, USA
b. Joint Institute for the Study of the Atmosphere and Ocean, University of Washington, Seattle, WA, USA
c. Pacific Marine Environmental Laboratory, National Oceanic and Atmospheric Administration, Seattle, WA, USA
d. Material Measurement Laboratory, Chemical Sciences Division, National Institute of Standards and Technology, Gaithersburg, MD, USA
+ Present address: Centre for Ocean and Atmospheric Sciences, School of Environmental Sciences, University of East Anglia, Norwich NR4 7TK, UK

***Corresponding author:** wcai@udel.edu

Keywords: Spectrophotometric pH measurement, meta-Cresol Purple (mCP), Dye perturbation

Abstract

Ocean acidification, a phenomenon of seawater pH decreasing due to increasing atmospheric CO_2, has a global effect on seawater chemistry, marine biology, and ecosystems. Ocean acidification is a gradual and global long-term process, the study of which demands high-quality pH data. The spectrophotometric technique is capable of generating accurate and precise pH measurements but requires adding an indicator dye that perturbs the sample original pH. While the perturbation is modest in well-buffered seawater, applications of the method in environments with lower buffer capacity such as riverine, estuarine, sea-ice meltwater and lacustrine environments are increasingly common, and uncertainties related to larger potential dye perturbations need further evaluation. In this paper, we assess the effect of purified meta-Cresol Purple (mCP) dye addition on the sample pH and how to correct for this dye perturbation. We conducted numerical simulations by incorporating mCP speciation into the MATLAB CO2SYS program to examine the changes in water sample pH caused by the dye addition and to reveal the

dye perturbation mechanisms. Then, laboratory experiments were carried out to verify the simulation results. The simulations suggest that the dye perturbation on sample pH is a result of total alkalinity (TA) contributions from the indicator dye and chemical equilibrium shifts that are related to both the water sample properties (pH, TA, and salinity) and the indicator dye solution properties (pH and solvent matrix). The laboratory experiments supported the simulation results; the same dye solution can lead to different dye perturbations in water samples with different pH, TA, and salinity values. The modeled adjustments agreed well with the empirically determined adjustments for salinities > 5, but it showed greater errors for lower salinities with disagreements as large as 0.005 pH units. Adjustments are minimized when the pH and salinity of the dye are matched to the sample. When the dye is used over a wide range of salinity, we suggest that it should be prepared in deionized water to minimize the dye perturbation effect on pH in the fresher sample waters with less well-constrained perturbation adjustments. We also suggest that the dye perturbation correction should be based on double dye addition experiments performed over a wide range of pH, TA, and salinity. Otherwise, multiple volume dye addition experiments are recommended for each sample to determine the dye perturbation adjustment. We further create a MATLAB function *dyeperturbation.m* that calculates the expected dye perturbation. This function can be used to validate empirically-derived adjustments or in lieu of empirical adjustments if dye addition experiments are unfeasible (e.g., for historical data). This study of dye perturbation evaluation and correction will improve the accuracy of the pH data, necessary for monitoring the long-term anthropogenic-driven changes in the seawater carbonate system.

1. Introduction

Atmospheric carbon dioxide (CO_2) has been dramatically increasing since the Industrial Revolution, mainly due to fossil fuel burning and deforestation (https://www.esrl.noaa.gov/gmd/ccgg/trends/). The increasing atmospheric CO_2 levels are tempered by the absorption of CO_2 by the ocean and the biosphere. However, oceanic CO_2 uptake causes ocean acidification, a seawater pH decreasing phenomenon (Doney et al., 2009). Ocean acidification has a vital effect on the seawater chemistry, marine organisms and global ecosystems (Orr et al., 2005; Doney et al., 2009; Cai et al., 2011;Andersson and Gledhill, 2013;

Waldbusser and Salisbury, 2014; Wanninkhof et al., 2015; Kwiatkowski and Orr, 2018; Landschützer et al., 2018). Ocean acidification is a subtle, long-term process, which requires high-quality data to better evaluate and understand it (Orr et al., 2018). The Global Ocean Acidification Observing Network (GOA-ON) suggested that the measurement of pH should achieve an accuracy of 0.02 pH units to assess *Weather* changes, i.e., spatial and short-term variations, while the *Climate* goal, focusing on deciphering decadal trends, requires pH data with an accuracy of 0.003 pH units.

The spectrophotometric pH method can be an accurate and precise technique for determining seawater pH (Lai et al., 2016; Liu et al., 2011; Ma et al., 2019; Mosley et al., 2004). This method relies on adding pH-sensitive indicator dye into water samples. Since the dye changes color with pH, the pH of the sample can be determined through absorbance spectra (Clayton and Byrne, 1993). There are many pH-sensitive indicator dyes available for spectrophotometric pH measurements, such as meta-Cresol Purple (mCP), thymol blue, and phenol red (Clayton and Byrne, 1993; Liu et al., 2011; Mosley et al., 2004; Patsavas et al., 2013; Soli et al., 2013; Zhang and Byrne, 1996). One of the most commonly used and well-characterized dyes for spectrophotometric pH measurements is mCP. Since Clayton and Byrne (1993) formalized spectrophotometric pH measurements for seawater using mCP, the reproducibility and accuracy of this method have been improved dramatically. The uncertainty sources of spectrophotometric pH measurements include factors such as dye perturbation, dye purity, instrument parameters (wavelength accuracy and absorbance errors), temperature control, pressure (DeGrandpre et al., 2014). The dye purity uncertainty has been addressed for mCP by purification through high-performance liquid chromatography (HPLC), and its physicochemical properties are now well characterized for a wide range of temperature, salinity (S), and pressure (Liu et al., 2011; Müller and Rehder, 2018a; Soli et al., 2013). Beyond these, an automated spectrophotometric system was designed (Carter et al., 2013) to achieve precise, reproducible and fast measurements with consistent temperature and pressure. These methodological improvements have enhanced the repeatability of spectrophotometric pH measurements to 0.0002 pH units (Liu et al., 2011) and decreased its combined uncertainty to 0.005–0.01 pH units (Bockmon and Dickson, 2015; Carter et al., 2013).

Despite recent improvements, our understanding of the pH perturbation caused by the dye addition remains limited. The characterization of mCP is performed in strongly buffered solutions, where the dye addition does not cause an appreciable pH perturbation of the buffer solution (Liu et al., 2011). But this is not the case in seawater or brackish samples. To correct the perturbation of sample pH due to dye addition, *The Guide to Best Practices for Ocean CO_2 Measurements* recommends a simple, empirical perturbation correction procedure by adding double volume indicator (Dickson et al., 2007). This procedure works well for open ocean waters using unpurified mCP. Chierici et al. (1999) also suggested an equation to correct for the dye perturbation effect on seawater sample pH based on both seawater sample pH and S, but this approach has not yet been widely applied to routine pH measurements and was developed before the properties of purified mCP were characterized over the full 0-40 S range. None of the recent research that used purified mCP clearly stated how much the addition of purified mCP would influence the measured sample pH over the full 0- 40 S range.

Clearly, there is room for improvement in quantifying the pH measurement uncertainty due to the dye perturbation, identifying the perturbation mechanism, and in establishing a strategy to reduce or even eliminate this source of uncertainty. We comprehensively evaluate the impact of dye perturbation using numerically simulated data and laboratory experiments in this paper. The numerical simulations were performed by adding the mCP acid-base speciation equations into the CO2SYS program (Lewis and Wallace, 1998; Van Heuven et al., 2011; Xu et al., 2017). The simulation results allow us to reveal the controlling chemical mechanisms on dye perturbation. We have also carried out laboratory experiments to verify the numerical simulation. Based on these results, we offer solutions regarding the mCP pH perturbation corrections for spectrophotometric pH measurements.

2. Theory and Method

2.1 Basic theory

The spectrophotometric pH measurements are based on the absorption spectra of samples with a pH-sensitive indicator dye. The dye, usually mCP, is a diprotic acid with acid and base forms that have distinct absorption peaks. In the pH range of natural seawater, mCP behaves as a monoprotic weak acid, so only its second dissociation constant needs to be taken into

consideration (Clayton and Byrne, 1993). In this case, the sample pH (on the total scale) (Dickson, 1993, 1984) can be estimated from the relative concentration of different mCP species and its second dissociation constant (Clayton and Byrne, 1993),

$$\mathrm{pH} = \mathrm{p}K_2 + log_{10}\frac{[\mathrm{I}^{2-}]}{[\mathrm{HI}^{-}]} \quad \text{(Equation 1)}$$

where $[HI^-]$ and $[I^{2-}]$ are the concentrations of the monoprotonated and unprotonated species of the indicator dye, respectively. The concentration ratio $[HI^-]/[I^{2-}]$ can be determined by the spectrophotometric measurements of the absorbance (A). Therefore, sample pH can be calculated as (Liu et al., 2011),

$$\mathrm{pH} = -\log(\mathrm{K}_2 e_2) + log_{10}(\frac{R - e_1}{1 - \frac{e_3}{e_2}R}) \quad \text{(Equation 2)}$$

where R is the absorbance ratio of mCP at λ_{578} and λ_{434}; e_1, e_2 and e_3 are the molar absorptivity ratios, $e_1 = \frac{578\varepsilon_{HI}}{434\varepsilon_{HI}}$, $e_2 = \frac{578\varepsilon_{I}}{434\varepsilon_{HI}}$, $e_3 = \frac{434\varepsilon_{I}}{434\varepsilon_{HI}}$.

To minimize the influence of dye addition to the sample pH, an empirical correction (Figure 1) was developed to determine the 'true pH' that would have been observed under no dye addition (Clayton and Byrne, 1993; Dickson et al., 2007). The empirical method relies on two assumptions. First, the change in R is linearly related to the volume of dye added (Figure 1, Step 1). Second, the changes in R per volume (mL) dye added ($\Delta R/\Delta V$) is a simple linear function of R (Equation 4). Following these two assumptions, the dye perturbation can be evaluated empirically based on double volume dye addition experiments. Some of the seawater samples are measured twice with different dye addition volumes to derive a relationship between absorbance changes and dye addition volume (Figure 1, Step 2). The first measurement is the absorbance ratio (R_1) of the seawater sample with a single addition of dye (V_1, mL), and the second absorbance ratio measurement (R_2) is performed after the second addition of dye to the same seawater sample (V_2, mL). The changes in R per milliliter of dye added ($\Delta R/\Delta V = (R_2 - R_1)/(V_2 - V_1)$) can be expressed as a function of R_1,

$$\frac{\Delta R}{\Delta V} = A + B \cdot R_1 \quad \text{(Equation 3)}$$

Then this relationship is applied to all the samples to obtain the theoretical R values without dye perturbation, being the empirically corrected absorbance ratio R_{EC} (Clayton and Byrne, 1993; Dickson et al., 2007). For any given sample, the measured R_1 can be corrected to R_{EC} as,

$$R_{EC} \equiv R_1 - \frac{\Delta R}{\Delta V} \cdot V_1 = R_1 - (A + B \cdot R_1) \cdot V_1 \quad \text{(Equation 4)}$$

$\Delta R/\Delta V$ determines how much R_1 should be empirically corrected to R_{EC} (Figure 1, Step 3). The pH value calculated from R_1 via Equation 2 is the seawater pH with the dye perturbation, while the pH value calculated from R_{EC} is considered as the 'true' seawater pH (Figure1, Step 4). The difference between the dye-perturbed pH and the 'true' pH is ΔpH. Some measurement approaches cannot reliably dispense precise volumes of dye and instead use changes in the absorbance at the mCP isosbestic wavelength as a proxy for the volume of dye added (Carter et al., 2013).

2.2 Numerical simulations of the dye perturbation

The pH perturbation caused by the dye addition can be calculated from the known equilibrium chemistry of seawater and the dye. For our calculation of the dye perturbation, we modified CO2SYS for MATLAB (Lewis and Wallace, 1998; Van Heuven et al., 2011; Xu et al., 2017) to a new function *dyeperturbation.m* (https://github.com/Sheenaxy/Dyeperturbation). The CO2SYS program is based on the equilibria of carbonate parameters, other weak acid-base species, and other seawater related chemistry parameters. Any two of the four carbonate parameters, total dissolved inorganic carbon (DIC), total alkalinity (TA), pH, and fugacity or partial pressure of CO_2 (fCO_2 or pCO_2), are chosen as inputs and the other two parameters can be calculated. Other input variables include the choices of equilibrium constants, temperature, pressure, S, the concentration of silicate and phosphate and the pH scale. In this work, we used DIC and TA pair to calculate pH.

In the CO2SYS, DIC is defined as the sum of $[HCO_3^-]$, $[CO_3^{2-}]$ and $[H_2CO_3]^*$ (by convention $[H_2CO_3]^*$ includes both aqueous CO_2 and H_2CO_3). TA is defined as the moles of hydrogen ion equivalent to the excess of proton acceptors over proton donors per kilogram of seawater (Dickson, 1981). The proton acceptors are bases formed from weak acids with pK $\geq$ 4.5 at 25 °C

and 0 mol/kg ionic strength, while the proton donors are acids with pK ≤ 4.5 at 25 °C and 0 mol/kg ionic strength. Thus, TA is defined as,

$$TA = CAlk + BAlk + [OH^-] + PAlk + SiAlk - [H^+]_{free} - [HSO_4^-] - [HF^-] \quad \text{(Equation 5)}$$

where CAlk is the carbonate alkalinity ($CAlk = [HCO_3^-] + 2[CO_3^{2-}]$); BAlk is the borate alkalinity ($BAlk = [B(OH)_4^-]$); PAlk is the phosphate alkalinity ($PAlk = [HPO_4^{2-}] + 2[PO_4^{3-}] - [H_3PO_4]$); and SiAlk is the silicate alkalinity ($SiAlk = [SiO(OH)_3^-]$). By solving Equation (5) iteratively we can calculate an equilibrium pH.

To test the influence of the dye addition in sample pH, we added the equilibria reactions of mCP as an additional chemical species into Equation 5. The two-step dissociation equilibria of mCP are,

$$H_2I = HI^- + H^+ \quad ; \quad K_1 = \frac{[HI^-][H^+]}{[H_2I]} \quad \text{(Equation 6)}$$

$$HI^- = I^{2-} + H^+ \quad ; \quad K_2 = \frac{[I^{2-}][H^+]}{HI^-} \quad \text{(Equation 7)}$$

K_1 is a function of temperature, where $\log K_1 = -782.62/T + 1.1131$ (Liu et al., 2011). When T = 298 K, $-\log K_1 = pK_1 = 1.5131$. K_2 is a function of S and temperature. Previous research considered $p(K_2e_2) = -\log_{10}(K_2e_2)$ as one term to simplify the mCP characterization process (Liu et al., 2011; Müller and Rehder, 2018b). Here we estimate K_2 as,

$$K_2 = \frac{10^{-(p(K_2e_2))}}{e_2} \quad \text{(Equation 8)}$$

$p(K_2e_2)$ varies from 7.6479 at S = 35, T = 298.15 K (Liu et al., 2011) to 8.2978 at S = 0, T = 298.15 K (Lai et al., 2016). Since there is no literature reference for the purified mCP e_2 function at the full S range (0 < S < 40), we linearly interpolated e_2 between S = 0 and S = 40 at T = 298.15 K using $e_2 = 2.306$ for T = 298.15 K, S= 0 (Lai et al., 2016), and $e_2 = 2.22$ for T = 298.15 K, S =35 (Clayton and Byrne, 1993) and linearly interpreted them between S=0 and 40 to simplify the calculation. Note that the e_2 value variation (from S = 0 to S =35 at T = 298.15 K) is small and has little influence on K_2 value calculated from $p(K_2e_2)$.

We define total concentration of indicator dye (TI) as, TI = $[I^{2-}]$ + $[HI^{-}]$ + $[H_2I]$. Therefore, the concentration of the different species of the indicator can be rewritten as,

$$[I^{2-}] = TI \cdot \frac{K_1K_2}{[H^+]^2+[H^+]K_1+K_1K_2} \quad \text{(Equation 9)}$$

$$[HI^{-}] = TI \cdot \frac{K_1[H^+]}{[H^+]^2+[H^+]K_1+K_1K_2} \quad \text{(Equation 10)}$$

$$[H_2I] = TI \cdot \frac{[H^+]^2}{[H^+]^2+[H^+]K_1+K_1K_2} \quad \text{(Equation 11)}$$

Similar to the carbonate system, the speciation of mCP varies with pH (Figure 2). For a given pH, we can calculate the concentration of each mCP form.

Knowing mCP dissociation constants and the species composition, we can calculate TA contributed by the indicator addition to the sample. The first dissociation constant K_1 of mCP is ~1.5 ($\leq$ 4.5), and the second dissociation constant is around 7.5 ($\geq$ 4.5) so the appropriate zero level of proton for mCP is HI^{-}. Thus, the TA of indicator dye solution (TA_I) can be calculated by,

$$TA_I = [I^{2-}]_I - [H_2I]_I + [OH^-] - [H^+]_{free}. \quad \text{(Equation 12)}$$

When the indicator solution is added to the seawater sample, it changes the TA of the sample. As TA mixes conservatively, the TA of a seawater sample with indicator (TA_m) is the mass-weighted mean TA of the seawater sample (TA_s) and that contributed by the indicator. Thus, TA_m becomes,

$$TA_m = \frac{m_s TA_s + m_I TA_I}{m_s+m_I} = CAlk + BAlk + [OH^-] + PAlk + SiAlk - [H^+]_{free} - [HSO_4^-] - [HF^-] + IAlk$$

(Equation 13)

where IAlk is the indicator dye alkalinity contributed by the mCP in the mixed solution. Note that IAlk is different from TA_I. Similar to CAlk, Balk and etc., IAlk is defined as,

$$IAlk = [I^{2-}]_m - [H_2I]_m = TI_m \cdot \frac{K_1K_2-[H^+]^2}{[H^+]^2+K_1[H^+]+K_1K_2} \quad \text{(Equation 14)}$$

TI_m is the indicator dye concentration in the mixing solution; $[I^{2-}]_m$ (calculated as Equation 9) and $[H_2I]_m$ (calculated as Equation 11) are the concentration of unprotonated and diprotonated mCP species in the mixing solution, respectively. By solving Equation (13) iteratively we can calculate a new equilibrium pH with the indicator dye addition. Note that since all chemical equilibria must be changed with the indicator dye solution addition, all TA components such as CAlk, BAlk, IAlk etc. will change too. We can, therefore, calculate the sample pH after adding the dye using Equation (13) and the original sample pH without dye perturbation using Equation (5). By subtracting the pH before dye addition, the pH changes due to dye addition can be calculated. The theoretical absorbance value R can be calculated from Equation (2) with known pH.

In our simulations, we set the pH and the concentration of the dye solution, dye/sample volume ratio to the values in the standard operating procedure (SOP) of *The Guide to Best Practices for Ocean CO_2 Measurements* (Dickson et al., 2007). We added 20 µL of 2.5 mmol/L mCP solution of pH = 8.0 to 15 mL sample (thus final dye concentration in the sample = 3.3 µmol/L). The SOP did not mention the S of the indicator solution. Here, we set the indicator solution S = 0 to match our laboratory experiments. In addition, we simulated the effect of dye perturbation under the dye solution S = 35 in Section 4.3.1.

The simulation was run with 50000 randomly chosen combinations of DIC and TA to reflect the ranges commonly found in the marine environment. TA is in the range of 300 to 2800 µmol kg^{-1} (bounding the open ocean TA range using a value appropriate for a low and high TA riverine endmember, respectively (Cai et al., 2008)); DIC is between 240 µmol kg^{-1} and 4200 µmol kg^{-1}; S is within 0–40. Although there is no general relationship among the chosen DIC, TA and S, we constrained the TA/DIC ratio to be within 0.8–1.5 to be more realistic for marine and estuarine environments. All simulations were performed under 25 °C. The selected dissociation constants, temperature, and pressure inputs are listed in Table 1. We also conducted three groups of simulation tests that match our laboratory experiments as described below.

2.3 Laboratory experimental design

Previous research suggested the effect of dye perturbation on sample pH is determined by the sample ionic strength and buffer capacity, yet this has not been experimentally demonstrated

(Chierici et al., 1999; Mosley et al., 2004). We designed three groups of laboratory experiments to verify the simulation results on dye perturbation (Figure 3). In the first group of experiments, we used water samples with fixed high S (36.3) and varying TA (about 1100 µmol kg^{-1}, 1450 µmol kg^{-1}, 2000 µmol kg^{-1}, 2350 µmol kg^{-1}). The second group of experiments was performed using water samples with fixed high TA (~2350 µmol kg^{-1}) and varied S (about 0, 4.8, 10, 15.5, 25.5, 36.3). The third group of experiments was performed using samples with fixed S-TA relationship (TA = 35.634 * S + 1377.1; S = 0, 12, 24, 36). In each group, we prepared two types of water and mixed them together to get four different TA-S pairs. Low S water originated from Mississippi and Atchafalaya river waters (both are of high TA, (Guo et al., 2012)). High S water is northern Gulf of Mexico seawater. Water was adjusted by additions of 0.2 mol/L NaOH or 0.2 mol/L HCl, which modify TA without significantly modifying S. The water was mixed to get different S or TA values along the gradient connecting the endmembers. Then, we adjusted the pH (and DIC) of these water samples by bubbling pure CO_2 gas or pure N_2 gas. TA was titrated with a ROSS™ combination electrode 8102 (Thermo Fisher Scientific) on a semi-automated open cell titrator (AS-ALK2, Apollo SciTech) and calibrated with certified reference material from Andrew G. Dickson's lab, Scripps Institution of Oceanography.

The pH of these water samples was measured spectrophotometrically. We prepared a 2.5 mmol/L indicator solution by dissolving purified mCP (from Robert H. Byrne's laboratory, University of South Florida) in deionized CO_2 free water. NaOH was added to adjust the indicator solution pH to ~8.0. The instrument setup and analysis procedure followed the design of Carter et al. (2013). We used an Agilent 8453 UV-visible spectroscopy system, a 48K-steps Kloehn pump controlled by a computer, a 10 cm flow-through cuvette with a water jacket, and a thermal controlled circulating water bath as described in Carter et al. (2013). The system was further automated to analyze a set of 8 water samples in sequence in about 40 minutes (AS-pH1, Apollo Scitech). All measurements were conducted at 25°C. We added 20 µL of 2.5 mmol/L purified mCP to 15 mL water sample as suggested by *The Guide to Best Practices for Ocean CO_2 Measurements* (Dickson et al., 2007). Measurement stability was checked with 2-amino-2-hydroxymethyl-1,3-propanediol (Tris) buffer solution (Batch #T33, from Andrew Dickson at Scripps Institution of Oceanography, University of California, San Diego). Every sample was measured by adding single-volume dye (20 µL) and double-volume dye (40 µL). Each sample was measured at least three times. We also conducted multiple dye addition experiments (adding

10 μL, 20 μL, 30 μL, 40 μL, 50 μL, and 60 μL of indicator) to some of these water samples to test the perturbation correction assumptions.

3. Results

3.1 Computer simulation results

3.1.1 Theoretical dye perturbation on the sample pH

We calculated pH from DIC, TA and S inputs with and without adding the indicator dye alkalinity term. Figure 4 shows that ΔpH (the water sample pH after a dye addition minus the water sample pH without the dye) is between 0 and 0.005 pH units for low-pH samples (~7.0–7.5), indicating the dye addition (S = 0, pH = 8.0) leads to an increase in the water sample pH. For sample pH higher than 7.5, ΔpH becomes negative, meaning the dye addition decreases the original sample pH. Intuitively, it would make sense if this transitional x-intercept value were located at the pH of the sample (in this case pH = 8.0). However, this is only the case for very-low salinity samples in Figure 4b. This is because when the low-ionic strength dye mixes with the high-ionic strength seawater, the speciation of the dye is shifted in favor of I^{2-} and protons are released (Müller and Rehder, 2018a). In Figure 4a, the absolute ΔpH of low-TA samples (dark blue dots) is larger than those of high-TA samples (red dots), showing the dye addition has a larger influence on the pH of low-TA samples. Figure 4b shows that sample S affects ΔpH values as well. The ΔpH of high-S samples (yellow dots, Figure 4b) changes less than that of low-S samples (dark blue dots, Figure 4b). Because both TA and S affect ΔpH, we made three extra groups of simulations to separate the effects of these two factors. The first group had fixed TA and variable S. The second group had fixed S and variable TA. The last group had a fixed TA-S relationship. The results of these simulations are shown together with the results from the laboratory experiments in Section 3.2.

3.1.2 Testing the assumptions of the empirical dye perturbation correction

As explained in Section 2.1, the empirical dye perturbation correction is based on two assumptions: (i) the absorbance ratio R changes linearly with the volume of dye added (or the change of R with dye addition volume is a constant), and (ii) the absorbance ratio change per mL dye addition ($\Delta R/\Delta V$) is a simple linear function of the absorbance ratio (R_1) with single volume

303 dye addition. We assessed the validity of these assumptions using our new MATLAB program
304 *dyeperturbation.m.*

305 To study the linearity between R and V, we calculated the sample pH with variable volumes of
306 dye additions from 1 µL to 100 µL. Then, the pH values were converted to the absorbance ratio
307 R based on Equation (2). Figure 5 shows the relationship between the dye addition volume and
308 the theoretical R, which is a simple linear relationship, and thus $\Delta R/\Delta V$ is a constant for each
309 DIC-TA pair. However, $\Delta R/\Delta V$ is not the same constant for every DIC-TA pair. When R is
310 smaller than 0.5 (referring to pH < 7.4), R is near constant or only slightly increases with
311 increasing dye volume. If R > 0.5, the $\Delta R/\Delta V$ has a negative slope against R. These results show
312 the first assumption is valid given a perfect spectrophotometer. Laboratory multiple dye addition
313 experiments also confirmed this conclusion derived from the simulation results (Figure 5b).

314 To test the second assumption, we evaluated the relationship between $\Delta R/\Delta V$ and R_1 and we
315 calculated the pH before and after single and double dye additions. Equation (2) was solved to
316 acquire R_1 and R_2, respectively. $\Delta R/\Delta V$ can be determined as the empirical correction method
317 suggests, $\Delta R/\Delta V = (R_2 - R_1)/(V_2 - V_1)$. The slope of the relationship between $\Delta R/\Delta V$ and R_1
318 changes depending on the sample properties. $\Delta R/\Delta V$ decreases faster (slower) with increasing R_1
319 under low (high) TA or S (Figure 6 -8). $\Delta R/\Delta V$ vs R_1 is strongly correlated, but not perfectly
320 linear, which may influence the calculation of the empirical corrected sample pH a little. The
321 $\Delta R/\Delta V$ decreasing rates in different TA or S samples will be discussed in detail in Section 3.2.

322 **3.2 Laboratory experiments results supporting model simulations**

323 To verify the simulation results, we conducted laboratory experiments using natural water from
324 the northern Gulf of Mexico, the Mississippi River and the Atchafalaya River. The endmember
325 waters were mixed to get various S and TA gradients as described in Section 2.3. The results of
326 the laboratory experiments are compared with those from computer simulations.

327 **3.2.1 Fixed S and varying TA group**

328 The $\Delta R/\Delta V$ and ΔpH values agree well between the simulations and the experimental results
329 under fixed high S (Figure 6). The simulation results demonstrate that the $\Delta R/\Delta V$ decreasing
330 rates with R_1 depend on the sample TA: $\Delta R/\Delta V$ of high-TA samples decreases with R_1 less than

that of low-TA samples (Figure 6a). The simulation results suggest that dye perturbation on high-TA samples (~2400 µmol kg^{-1}) pH is rather small (-0.0013 – 0.0005 pH units; Figure 6b). When sample TA is lowest (~1100 µmol kg^{-1}), dye perturbation effect on ΔpH is the largest at about -0.0030 to 0.0016 pH units (dark blue line in Figure 6b).

In the experimental results, ΔR/ΔV decreases less with increasing R_1 when sample TA is high (~2400 µmol kg^{-1}); and ΔR/ΔV decreases more rapidly when sample TA is low (~1100 µmol kg^{-1}). Based on Figure 6c, we made a simple linear regression of ΔR/ΔV against R_1 for each TA group and calculated the ΔpH (Figure 6d) using Equations (3) and (4). Experimental results (Figure 6d) are similar to the simulation results (Figure 6b); dye perturbation increases with sample pH increasing and TA decreasing. In Figure 6d, the ΔpH for high-TA samples (~2400 µmol kg^{-1}) is closer to 0 (-0.001– 0.000 pH units) compared to ΔpH for low-TA samples (~1100 µmol kg^{-1}). Laboratory results support the simulation results (Figure 9). Therefore, for high salinity samples, the differences between simulated ΔR/ΔV - experimental ΔR/ΔV (Δ(ΔR/ΔV)) is close to 0 with a 0.06 standard deviation. The simulated ΔpH and the experimental ΔpH are very close to each other with average Δ(ΔpH) 0.0008 (blue square dots in Figure 9b).

3.2.2 Fixed TA and varying S group

Since Mississippi river water has the same high TA (~2350 µmol kg^{-1}) as the northern Gulf of Mexico seawater, we can obtain a series of samples with the same high TA but distinct S by mixing these two types of water in different ratios. Our simulation shows the decrease in ΔR/ΔV with R_1 is minimized (relative to low S sample) when sample S is high (Figure 7a). The experimental results support the simulation results (Figure 7a,7c and 9a): when S = 36, ΔR/ΔV decreases to -0.2 at R_1 = 1.9. When S = 0, ΔR/ΔV decreases to -0.8 at R_1 = 1.5. Both simulation results (Figure 7b) and experimental results (Figure 7d) show the dye perturbation on sample pH is large in low-S water, while the perturbation is small in high-S water. In terms of ΔpH, the experimental and simulated results match well when water sample S >5 (Figure 9b). However, when sample salinity equals zero and pH is low, the experimental and simulated perturbation results have obvious difference (orange cross dots in red circle, Figure 9b). This could be both the uncertainties in the spectrophotometric pH measurements and in the carbonate constants used

in the theoretical calculations at low S (S<5) that may contribute to the mismatch of theory and observation.

3.2.3 Fixed TA and S relationship group

The last scenario is mixing low-TA and low-S water with high-TA and high-S water in different ratios to obtain a series of TA-S gradient water. This case is representative of natural waters in most estuarine and coastal areas, where river TA is much lower than seawater TA and that TA and S have a linear relationship during mixing. Simulation results (Figure 8a) show that $\Delta R/\Delta V$ decrease little with increasing R_1 in highly saline and alkaline water with S = 36 and TA = 2800 μmol kg^{-1}, while $\Delta R/\Delta V$ decreases rapidly with R_1 in the fresh riverine water of S = 0 and TA = 1100 μmol kg^{-1}. The relationship between $\Delta R/\Delta V$ and R_1 is nearly linear when $R_1 > 0.5$. As for ΔpH, the dye perturbation on sample pH is very small (-0.0015 – 0.001 pH units) for S = 36 and TA = 2800 μmol kg^{-1}, while it is large (-0.01– 0.003 pH units) for low-S and low-TA water (Figure 8b, blue line). The experimental results (Figure 8c and 8d) agree with the simulation results (Figure 8a, 8b and Figure 9). Both of them show that dye perturbation presents little influence on $\Delta R/\Delta V$ and sample pH in high-S and high-TA samples. Except for the water of S = 0, the relationship of $\Delta R/\Delta V$ vs. R_1 can be considered as linear (Figure 8c) when $R_1 > 0.5$. The average difference between simulated ΔpH and experimental ΔpH is -0.0006, indicated by yellow dots in Figure 9b.

4. Discussion

4.1 The mechanism of dye perturbation

The addition of mCP can perturb the original sample pH by (i) modification of the water sample TA, and (ii) H^+ redistribution in the solution. The contribution of extra TA can be calculated from the indicator solution properties. We simulated the addition of 20 μL (or 50 μmol) mCP solution (2.5 mmol/L, S = 0, pH = 8) to 15 mL high-S seawater sample at 25 °C. Under these conditions, the added $[H^+]$, $[OH^-]$, and the total mole concentration of mCP solution would be diluted 750 times. Thus, the total concentration of mCP in the water sample is about 3.33 μmol/L. The mCP solution is a mixture of H_2I, I^{2-} and HI^-. The mCP solution (pH = 8.0, S=0)

mainly contributes ~20 % I^{2-} and ~80 % HI^{-} to the seawater sample (Figure 2). The added HI^{-} does not affect the water sample TA, since HI^{-} is the zero level of proton in the titration. The TA of the indicator dye solution is $TA_I = [I^{2-}]_I - [H_2I]_I + [OH^-] - [H^+]_{free}$. After mixing the indicator dye and the water sample, the sample will have mCP species in solution and a new TA that is the mass-weighted average alkalinity of the indicator solution TA_I and the original water sample TA, $TA_m = (m_s TA_s + m_I TA_I)/(m_s + m_I))$. When the original water sample TA_s is high, the capacity of the sample resisting extra TA addition is high as well. Thus, the effect of indicator addition perturbation is smaller for high-TA samples than for low-TA samples.

The addition of the HI^{-} - I^{2-} pair can change the sample original pH by H^+ exchange between the sample solution and the dye. The H^+ redistributes among all the chemical species including carbonate, boron, and phosphate as well as the HI^{-} - I^{2-} pair. Then, a new chemical equilibrium is established, in which the TA and I^{2-} contributed by mCP plays a role. The addition of the free H^+ and OH^- initially present in the indicator solution is small enough to be neglected. The exchange of H^+ that occurs among different chemical species and the solution can be significant if the indicator solution encounters a vastly different TA or pH environment. Beyond TA and pH, the exchange and redistribution of H^+ is also influenced by the sample S. When the mCP dye is added to a sample that has very different S from that of the indicator solution, the pK values of mCP shift dramatically and H^+ transfers among different acid-base species. Thus, the dye perturbation can be the result of dissociation coefficients changes. Overall, the influence of the dye perturbation is determined by the S, TA, and pH of the water samples and the mCP solution.

4.2 pH bias caused by the empirical correction method

Our experiments results show that the dye perturbation magnitude is distinct in different S and TA samples. Therefore, the method for empirical dye perturbation correction, which does not take the properties of samples into account, needs careful re-evaluation when applied to water samples spanning a large range of properties. In this section, we assess several common biases that are caused by applying the empirical dye perturbation correction.

4.2.1 One dye perturbation curve for all samples

Applying a unique dye perturbation curve (one linear regression for $\Delta R/\Delta V$ vs. R_1) to a series of samples with different TA and S can lead to biases (Figure 10a, black vs. blue vs. yellow line) because the change of $\Delta R/\Delta V$ vs. R_1 is not constant with changing TA and S. If only one averaged linear regression of $\Delta R/\Delta V$ vs. R_1 (as the black line in Figure 10a indicates) is made for all samples (S = 0–40, TA = 1100 µmol kg^{-1} – 2800 µmol kg^{-1}), the samples with high S and high TA are about 0 – 0.001 pH overcorrected (yellow arrows in Figure 10a and 10b). On the contrary, the dye perturbation influence on low-S and low-TA samples (as the blue line and arrow indicates in Figure 10a) should be larger than that calculated from the averaged $\Delta R/\Delta V$ vs. R_1 regression line. For a sample with low S and low TA (S = 0, TA = 1100 µmol kg^{-1}), the corrected pH from average $\Delta R/\Delta V$ vs. R_1 regression line is about 0.001–0.006 pH units is under-corrected or is smaller than it should be (blue arrows, Figure 10b).

4.2.2 Insufficient double dye addition samples over a wide range of pH

If the double dye addition samples only fall in a very narrow pH range, the dye perturbation correction bias can be very large when the average $\Delta R/\Delta V$ vs. R_1 regression line is extrapolated to extreme pH (Figure 10a, red line). For example, if water samples are from a coastal cruise, the samples may cover a wide S and TA range (S = 0– 40, TA = 1100 –2800 µmol kg^{-1}). However, if the double dye addition samples insufficiently cover the pH range of the field samples (only in the range of R = 1.0 ~ 1.5, as figure 10a red solid line shows), then $\Delta R/\Delta V$ to R_1 slope will decrease far more than the actual sample slope. The $\Delta R/\Delta V$ of high-S and high-TA samples (S = 40, TA = 2800 µmol kg^{-1}) from the extrapolation line (figure 10a, red dash line) is much smaller than its theoretical values at high pH (Figure 10a, red arrow), which can cause an overcorrection of 0.005 pH units (Figure 10b, right red arrow). For the low S and low TA samples (S = 0, TA = 1100 µmol kg^{-1}), the $\Delta R/\Delta V$ from extrapolation is larger than its theoretical value at low pH, and the pH correction is 0.002 pH units smaller than its theoretical value (left red arrows in Figures 10a and 10b). It is therefore important to ensure that the lines are fit based to dye-addition experiment data from a set of samples that is representative of the measurements.

The above discussions do not include possible human errors that can lead to enormous dye perturbation correction errors. In our initial tests, we added 30 µL stock solution (2.5 mmol/L) to 15 mL sample for the sample measurement and 60 µL mCP stock solution for the double dye

addition experiment. In the double dye addition test, the final mCP concentration in the sample solution was too high (~10 µmol/L), which caused the absorbance peak values in double dye addition experiments to exceed the linear range of the Agilent 8453 instrument. This introduced an erroneous ΔpH correction as large as 0.01, at least twice as larger as the true correction value. Such errors should be avoided in the dye perturbation experiments. The final mCP concentration in the sample should always fall in the range of linear detection range. Since pH data literatures do not generally report their double dye correction information, it is difficult to evaluate the extent of this error. However, we caution field workers to check if their double addition is still within the analytical linear range of the instrument if the experimentally derived double dye correction is suspiciously large. We further note that the negative bias visible in Figure 9a (average $\Delta(\Delta R/\Delta V)$ = -0.0008) could be attributed to a non-linear response in one wavelength vs. another (i.e., the I^{2-} peak at 578 nm may not increase with increasing dye concentration to the same degree as the HI^{-} at 434 nm). For most samples, this results in small errors in the empirical adjustments, but for others (e.g., the 3 circled Fixed TA group points in Figure 9b) the impact of these errors on pH can be significant. Alternately, a negative $\Delta(\Delta R/\Delta V)$ bias could be explained if the dye pH were lowered by the dye gradually absorbing CO_2.

4.3 Reduction of dye perturbation

4.3.1 The optimization of dye solution preparation

The preparation of the dye solution is very important because it is directly related to the magnitude of the dye perturbation. The purified mCP solid is in the form of H_2I, which is very hard to dissolve in the water. Adding NaOH to the solvent can help with the dissolution and adjust the mCP indicator pH. Since the natural seawater pH falls in the range of 7.4 – 8.5, the recommended dye pH is about 7.9 ± 0.1 pH (SOP 6b, (Dickson et al., 2007)). However, the amount of added NaOH is different for deionized water and 0.7 mol/L NaCl (S =35) solution. In the 0.7 mol/L NaCl, the ionic strength is high, and the mCP pK_2 value is smaller than it is in the deionized water, (Müller and Rehder, 2018a) which means more I^{2-} is needed to keep the same pH (Equation1). Therefore, more NaOH should be added to the stock solution to produce more I^{2-}, thus contributing more TA to the water sample.

When purified mCP is used for open ocean spectrophotometric seawater pH measurements, it is common to dissolve the indicator in 0.7 mol/L NaCl solution and adjust the pH to approximately 8.0. The perturbation effect of this indicator solution is very small for high S-TA seawater sample, and the perturbation is near 0 when the sample pH is close to 8.0 (Figure 11b). However, this indicator solution is not ideal for low S samples (e.g., brackish or riverine water sample (blue dots, Figure 11b)). The shift of pK_2 per unit salinity is the largest at very low ionic strength (Müller and Rehder, 2018b). When this S =35, pH = 8.0 mCP indicator is added to the low S water sample, the pK_2 increase is quite significant even though the dye is diluted by a much larger volume of sample. This pK_2 change causes a greater pH perturbation for applying high S stock solutions to low S sample than applying low S stock solution to high S samples (Figure 11, low-S blue dots).

In addition, we should be cautious when using the S = 35 and pH = 8.0 indicator to measure high-S and low-pH seawater samples (e.g., deep seawater measured at T = 25 °C) because the second assumption of the empirical dye perturbation correction method, $\Delta R/\Delta V$ vs. R_1 having linear relationship, is no longer valid (especially when R close to 0.5, Figure 11a). The non-linearity at low pH results is the result of the R ratio being defined with the absorbance associated with the acidic form of mCP in the denominator. This amplifies R changes at high pH and diminishes R changes at low pH. To avoid the non-linear part of the $\Delta R/\Delta V$ vs. R_1 relationship, we can choose to use a S=35 and pH less than 8 indicator dye solution or to use a S = 0 and pH = 8.0 indicator dye solution (that has a more linear response over the entire pH range, Figure 10a, 11a).

Overall, the preparation of the dye solution should be based on the expected sample S, pH, and TA. The goal is to achieve a minimum dye perturbation around the sample original pH. We provide a new MATLAB program to determine the pH and S of the indicator solution that will produce the lowest pH perturbation. An example is provided in the supplementary material.

4.3.2 Practical method for dye perturbation correction

The empirical dye perturbation correction method is limited because it does not take the sample S and TA into consideration when performing the double dye addition experiments. Chierici et al. (1999) took S into consideration, but not TA, when applying the indicator addition

perturbation correction. In this paper, both experimental and computational results suggest that the dye perturbation is smaller for high-TA and high-S samples than that for low-TA and low-S samples. Here, we suggest that the selection of double dye addition samples should cover as wide range of S, TA and pH as the collection of water samples analyzed, and the regression line for $\Delta R/\Delta V$ vs. R_1 should be made separately for different S and TA groups. Otherwise, it will be difficult to well define the $\Delta R/\Delta V$ vs. R_1 regression line, which may cause the biases discussed in Section 4.2.

Another method to eliminate dye perturbation is an empirical extrapolation of R to zero dye addition for every individual sample (Lai et al., 2016). This method can remove the effect of S and TA influence of the sample. Simulation results (Figure 5a) indicate that for a single sample, R and volume of dye added (concentration) have a simple linear relationship. We verified the simulation results with the laboratory experiments (Figure 5b). Therefore, it is practical to linearly extrapolate the R to zero dye addition for each sample. Previous research suggested that for freshwater or low-S samples, dye perturbation on sample pH should be determined for every sample to obtain the best accuracy due to the low buffer capacity of freshwater (Lai et al., 2016; Moseley, 2004). For seawater, even though the buffer capacity is much higher than that of freshwater, we still suggest performing multiple volume dye addition experiments to all the samples when not enough samples covering different S and TA are available. This approach has the limitations that (1) random errors in individual dye-addition experiment measurements can be erroneously extrapolated unless the experiment is repeated enough times to adequately characterize the dye perturbation response and (2) that this requires more analysis time, dye, and sample.

If experiments for dye perturbation correction cannot be performed, we provide a new MATLAB function that can calculate the theoretical dye perturbation. With known sample properties (TA, DIC, S and T), indicator dye properties (pH, S, concentration) and sample/dye mixing volume ratios, the dye perturbation on sample pH can be calculated. The function (*dyeperturbation.m*) details and an example result are provided in the Supplementary Material.

5. Conclusions

The addition of mCP solution to water samples changes the sample TA composition and redistributes hydrogen ion among other chemical equilibrium parameters. The effect of this dye perturbation is distinct for water samples with different TA, S, and pH; and it also depends on the mCP solution preparation. To determine the "true pH" of the water sample without a dye perturbation, a correction for the dye perturbation is needed, which is very important for low-buffered, low-S and low-TA samples. This work not only reveals the mechanism by which the dye affects the carbonate parameters of the seawater samples, but also allows improving the accuracy of spectrophotometric pH measurements. The high-quality data will help with identifying small decadal pH changes and give a better understanding of ocean acidification.

The empirical method of dye perturbation correction based upon a single regression is limited and may cause biases on corrected pH (biases of ~0.001–0.005 pH units). We suggest taking TA and S of the analyzed samples into consideration when selecting the samples to perform the double dye addition for the empirical method of dye perturbation correction method. If the number of samples is low or the samples do not cover a wide range of TA, S and pH, a better way to eliminate the dye perturbation is studying the dye perturbation through multivolume dye additions to each sample, ideally repeated multiple times to minimize the effects of random errors. We also provide a new MATLAB function that helps calculate theoretical dye perturbations, which can be used as a sanity check for dye perturbation adjustments or use it in lieu of an empirical adjustment. The function is validated by empirical measurements, but considerable uncertainties remain in low salinity sample due to uncertainties in carbonate chemistry and mCP speciation coefficients.

Acknowledgement:

We thank Yuanyuan Xu, Ouyang Zhangxian for helpful discussions in this work. We thank Najid Hussain for helping with the experiments. This work was supported by National Oceanic and Atmospheric Administration (NOAA)'s Ocean Acidification Program via award: NA17OAR0170332 to WJC. The authors would like to thank Dr. Michael R. Winchester and Dr. Ashley B. Green (NIST Materials Measurement Laboratory) for their helpful reviews. These are JISAO and PMEL contribution numbers 2020-1075 and 5113, respectively. We also would like

to thank the insightful comments from 2 anonymous reviewers. Certain commercial equipment or materials are identified in this paper to specify adequately the experimental procedure. Such identification does not imply recommendation or endorsement by the National Institute of Standards and Technology or the National Institutes of Health, nor does it imply that the materials or equipment identified are necessarily the best available for the purpose.

Table 1. Constant choices for CO2SYS calculation.

Parameters	**Choices**
Carbonate Dissociation Constants K_1, K_2	(Millero et al., 2010)
Dissociation constants of HSO_4^-, KSO_4	(Dickson, 1990a)
Dissociation constants of F, KF	(Dickson and Riley, 1979)
Dissociation constants of B, KB	(Dickson, 1990b)
Sulfate Concentration	(Morris and Riley, 1966)
Fluoride Concentration	(Riley, 1965)
Boron Concentration	(Uppström, 1974)

566

567 **References:**

568 Andersson, A.J., Gledhill, D., 2013. Ocean Acidification and Coral Reefs: Effects on
569 Breakdown, Dissolution, and Net Ecosystem Calcification. Ann. Rev. Mar. Sci. 5, 321–348.
570 https://doi.org/10.1146/annurev-marine-121211-172241

571 Bockmon, E.E., Dickson, A.G., 2015. An inter-laboratory comparison assessing the quality of
572 seawater carbon dioxide measurements. Mar. Chem. 171, 36–43.
573 https://doi.org/10.1016/j.marchem.2015.02.002

574 Cai, W.-J., Wang, Y., Hodson, R.E., 1998. Acid-Base Properties of Dissolved Organic Matter in
575 the Estuarine Waters of Georgia, USA. Geochim. Cosmochim. Acta 62, 473–483.
576 https://doi.org/10.1016/S0016-7037(97)00363-3

577 Cai, W.J., Guo, X., Chen, C.T.A., Dai, M., Zhang, L., Zhai, W., Lohrenz, S.E., Yin, K.,
578 Harrison, P.J., Wang, Y., 2008. A comparative overview of weathering intensity and
579 HCO3- flux in the world's major rivers with emphasis on the Changjiang, Huanghe,
580 Zhujiang (Pearl) and Mississippi Rivers. Cont. Shelf Res. 28, 1538–1549.
581 https://doi.org/10.1016/j.csr.2007.10.014

582 Cai, W.J., Hu, X., Huang, W.J., Murrell, M.C., Lehrter, J.C., Lohrenz, S.E., Chou, W.C., Zhai,
583 W., Hollibaugh, J.T., Wang, Y., Zhao, P., Guo, X., Gundersen, K., Dai, M., Gong, G.C.,
584 2011. Acidification of subsurface coastal waters enhanced by eutrophication. Nat. Geosci.
585 4, 766–770. https://doi.org/10.1038/ngeo1297

586 Carter, B.R., Radich, J.A., Doyle, H.L., Dickson, A.G., 2013. An automated system for
587 spectrophotometric seawater pH measurements. Limnol. Oceanogr. Methods 11, 16–27.
588 https://doi.org/10.4319/lom.2013.11.16

589 Chierici, M., Fransson, A., Anderson, L.G., 1999. Influence of m-cresol purple indicator
590 additions on the pH of seawater samples: Correction factors evaluated from a chemical
591 speciation model. Mar. Chem. 65, 281–290. https://doi.org/10.1016/S0304-4203(99)00020-
592 1

593 Clayton, T.D., Byrne, R.H., 1993. Spectrophotometric seawater pH measurements : total
594 hydrogen results. Deep. Res. 40, 2115–2129. https://doi.org/10.1016/0967-0637(93)90048-
595 8

596 DeGrandpre, M.D., Spaulding, R.S., Newton, J.O., Jaqueth, E.J., Hamblock, S.E., Umansky,
597 A.A., Harris, K.E., 2014. Considerations for the measurement of spectrophotometric pH for
598 ocean acidification and other studies. Limnol. Oceanogr. Methods 12, 830–839.
599 https://doi.org/10.4319/lom.2014.12.830

600 Dickson, A.G., 1993. The measurement of sea water pH. Mar. Chem. 44, 131–142.
601 https://doi.org/10.1016/0304-4203(93)90198-W

602 Dickson, A.G., 1990a. Standard potential of the reaction: AgCl(s) + 1 2H2(g) = Ag(s) + HCl(aq),
603 and and the standard acidity constant of the ion HSO4- in synthetic sea water from 273.15
604 to 318.15 K. J. Chem. Thermodyn. https://doi.org/10.1016/0021-9614(90)90074-Z

605 Dickson, A.G., 1990b. Thermodynamics of the dissociation of boric acid in synthetic seawater
606 from 273.15 to 318.15 K. Deep Sea Res. Part A, Oceanogr. Res. Pap.
607 https://doi.org/10.1016/0198-0149(90)90004-F

608 Dickson, A.G., 1984. pH scales and proton-transfer reactions in saline media such as sea water.
609 Geochim. Cosmochim. Acta. https://doi.org/10.1016/0016-7037(84)90225-4

610 Dickson, A.G., 1981. An exact definition of total alkalinity and a procedure for the estimation of
611 alkalinity and total inorganic carbon from titration data. Deep Sea Res. Part A, Oceanogr.
612 Res. Pap. https://doi.org/10.1016/0198-0149(81)90121-7

613 Dickson, A.G., Riley, J.P., 1979. The estimation of acid dissociation constants in seawater media
614 from potentionmetric titrations with strong base. I. The ionic product of water - Kw. Mar.
615 Chem. https://doi.org/10.1016/0304-4203(79)90001-X

616 Dickson, A.G., Sabine, C.L., Christian, J.R., 2007. Guide to best practices for ocean CO2
617 measurements. North Pacific Marine Science Organization.

618 Doney, S.C., Fabry, V.J., Feely, R.A., Kleypas, J.A., 2009. Ocean Acidification: The Other CO 2

619 Problem. Ann. Rev. Mar. Sci. 1, 169–192.
620 https://doi.org/10.1146/annurev.marine.010908.163834

621 Guo, X., Cai, W., Huang, W., Wang, Y., Chen, F., Murrell, M.C., Lohrenz, S.E., Jiang, L., Dai,
622 M., Hartmann, J., Lin, Q., Culp, R., 2012. Carbon dynamics and community production in
623 the Mississippi River plume 57, 1–17. https://doi.org/10.4319/lo.2012.57.1.0001

624 Kwiatkowski, L., Orr, J.C., 2018. Diverging seasonal extremes for ocean acidification during the
625 twenty-first centuryr. Nat. Clim. Chang. 8, 141–145. https://doi.org/10.1038/s41558-017-
626 0054-0

627 Lai, C.Z., DeGrandpre, M.D., Wasser, B.D., Brandon, T.A., Clucas, D.S., Jaqueth, E.J., Benson,
628 Z.D., Beatty, C.M., Spaulding, R.S., 2016. Spectrophotometric measurement of freshwater
629 pH with purified meta-cresol purple and phenol red. Limnol. Oceanogr. Methods 14, 864–
630 873. https://doi.org/10.1002/lom3.10137

631 Landschützer, P., Gruber, N., Bakker, D.C.E., Stemmler, I., Six, K.D., 2018. Strengthening
632 seasonal marine CO2 variations due to increasing atmospheric CO2. Nat. Clim. Chang. 8.
633 https://doi.org/10.1038/s41558-017-0057-x

634 Lewis, E., Wallace, D., 1998. Program developed for CO2 system calculations. Ornl/Cdiac-105.
635 https://doi.org/4735

636 Liu, X., Patsavas, M.C., Byrne, R.H., 2011. Purification and characterization of meta-cresol
637 purple for spectrophotometric seawater ph measurements. Environ. Sci. Technol. 45, 4862–
638 4868. https://doi.org/10.1021/es200665d

639 Ma, J., Shu, H., Yang, B., Byrne, R.H., Yuan, D., 2019. Spectrophotometric determination of pH
640 and carbonate ion concentrations in seawater: Choices, constraints and consequences. Anal.
641 Chim. Acta 1081, 18–31. https://doi.org/10.1016/j.aca.2019.06.024

642 Millero, F.J., Graham, T.B., Huang, F., Bustos-Serrano, H., Pierrot, D., 2006. Dissociation
643 constants of carbonic acid in seawater as a function of salinity and temperature. Mar. Chem.
644 https://doi.org/10.1016/j.marchem.2005.12.001

645 Morris, A.W., Riley, J.P., 1966. The bromide/chlorinity and sulphate/chlorinity ratio in sea
646 water. Deep. Res. Oceanogr. Abstr. https://doi.org/10.1016/0011-7471(66)90601-2

647 Mosley, L.M., Husheer, S.L.G., Hunter, K.A., 2004. Spectrophotometric pH measurement in
648 estuaries using thymol blue and m-cresol purple. Mar. Chem. 91, 175–186.
649 https://doi.org/10.1016/j.marchem.2004.06.008

650 Müller, J.D., Rehder, G., 2018a. Metrology of pH Measurements in Brackish Waters—Part 2:
651 Experimental Characterization of Purified meta-Cresol Purple for Spectrophotometric pHT
652 Measurements. Front. Mar. Sci. 5, 1–9. https://doi.org/10.3389/fmars.2018.00177

653 Müller, J.D., Rehder, G., 2018b. Metrology of pH Measurements in Brackish Waters—Part 2:
654 Experimental Characterization of Purified meta-Cresol Purple for Spectrophotometric pHT
655 Measurements. Front. Mar. Sci. 5, 1–9. https://doi.org/10.3389/fmars.2018.00177

656 Orr, J.C., Epitalon, J.M., Dickson, A.G., Gattuso, J.P., 2018. Routine uncertainty propagation for
657 the marine carbon dioxide system. Mar. Chem. 207, 84–107.
658 https://doi.org/10.1016/j.marchem.2018.10.006

659 Orr, J.C., Fabry, V.J., Aumont, O., Bopp, L., Doney, S.C., Feely, R.A., Gnanadesikan, A.,
660 Gruber, N., Ishida, A., Joos, F., Key, R.M., Lindsay, K., Maier-Reimer, E., Matear, R.,
661 Monfray, P., Mouchet, A., Najjar, R.G., Plattner, G.-K., Rodgers, K.B., Sabine, C.L.,
662 Sarmiento, J.L., Schlitzer, R., Slater, R.D., Totterdell, I.J., Weirig, M.-F., Yamanaka, Y.,
663 Yool, A., 2005. Anthropogenic ocean acidification over the twenty-first century and its
664 impact on calcifying organisms. Nature 437, 681–686. https://doi.org/10.1038/nature04095

665 Patsavas, M.C., Byrne, R.H., Liu, X., 2013. Purification of meta-cresol purple and cresol red by
666 flash chromatography: Procedures for ensuring accurate spectrophotometric seawater pH
667 measurements. Mar. Chem. 150, 19–24. https://doi.org/10.1016/j.marchem.2013.01.004

668 Riley, J.P., 1965. The occurrence of anomalously high fluoride concentrations in the North
669 Atlantic. Deep. Res. Oceanogr. Abstr. https://doi.org/10.1016/0011-7471(65)90027-6

670 Screening, T., Lecture, C., n.d. Nakamura_Harned_Cells 36–41.

671 Soli, A.L., Pav, B.J., Byrne, R.H., 2013. The effect of pressure on meta-Cresol Purple
672 protonation and absorbance characteristics for spectrophotometric pH measurements in
673 seawater. Mar. Chem. 157, 162–169. https://doi.org/10.1016/j.marchem.2013.09.003

674 Uppström, L.R., 1974. The boron/chlorinity ratio of deep-sea water from the Pacific Ocean.
675 Deep. Res. Oceanogr. Abstr. https://doi.org/10.1016/0011-7471(74)90074-6

676 Van Heuven, S., Pierrot, D., Rae, J.W.B., Lewis, E., Wallace, D.W.R., 2011. MATLAB Program
677 Developed for CO2 System Calculations. ORNL/CDIAC-105b.
678 https://doi.org/10.3334/CDIAC/OTG.CO2SYS_MATLAB_V1.1

679 Waldbusser, G.G., Salisbury, J.E., 2014. Ocean Acidification in the Coastal Zone from an
680 Organism's Perspective: Multiple System Parameters, Frequency Domains, and Habitats.
681 Ann. Rev. Mar. Sci. 6, 221–247. https://doi.org/10.1146/annurev-marine-121211-172238

682 Xu, Y.Y., Pierrot, D., Cai, W.J., 2017. Ocean carbonate system computation for anoxic waters
683 using an updated CO2SYS program. Mar. Chem. 195, 90–93.
684 https://doi.org/10.1016/j.marchem.2017.07.002

685 Zhang, H., Byrne, R.H., 1996. Spectrophotometric pH measurements of surface seawater at in-
686 situ conditions: Absorbance and protonation behavior of thymol blue. Mar. Chem. 52, 17–
687 25. https://doi.org/10.1016/0304-4203(95)00076-3

688

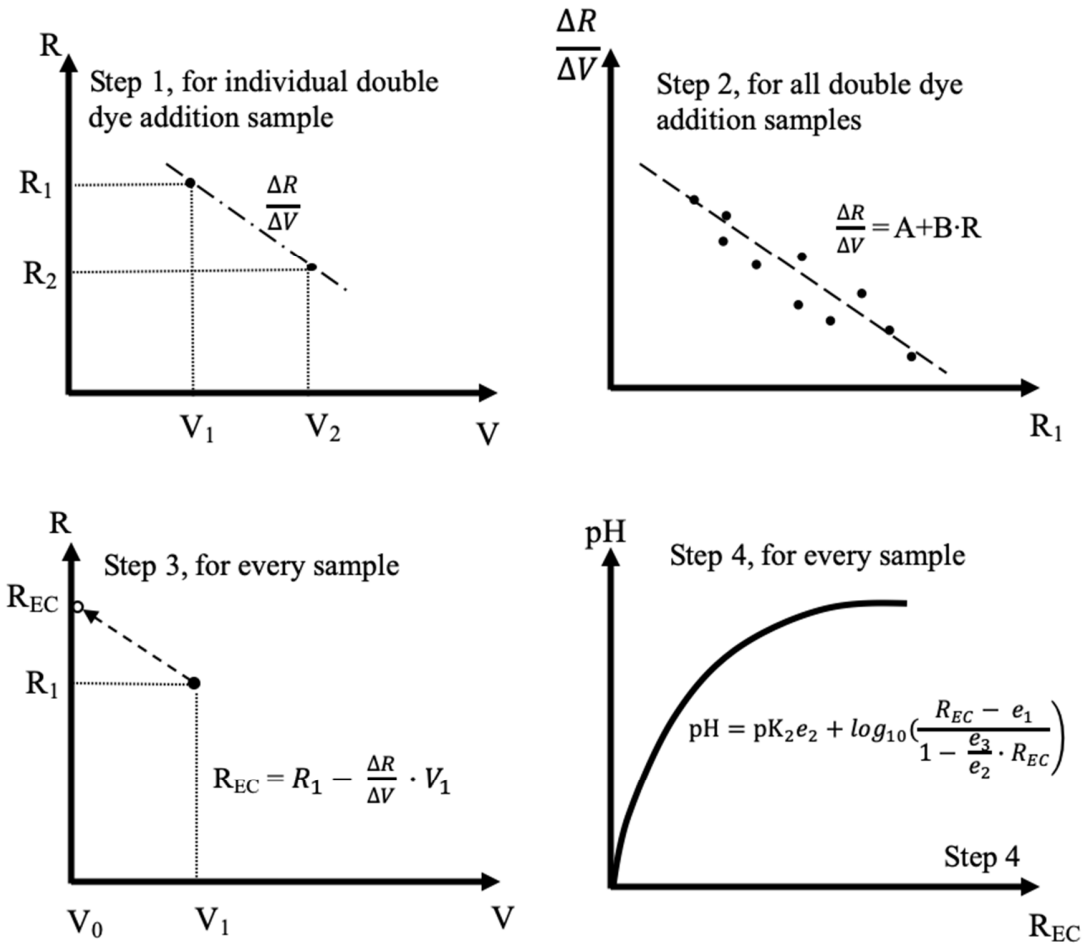

Figure 1. Four steps of empirical dye perturbation. Step 1, calculate $\frac{\Delta R}{\Delta V}$ from limited number of double dye addition experiments. Step 2, plot $\frac{\Delta R}{\Delta V}$ against R_1 to get a regression linear relationship. The first 2 steps are the empirical dye perturbation assumptions. Step 3, apply extrapolated $\frac{\Delta R}{\Delta V}$ to every sample to get R_{EC}. Step4, use R_{EC} to calculate sample 'true' pH without dye addition.

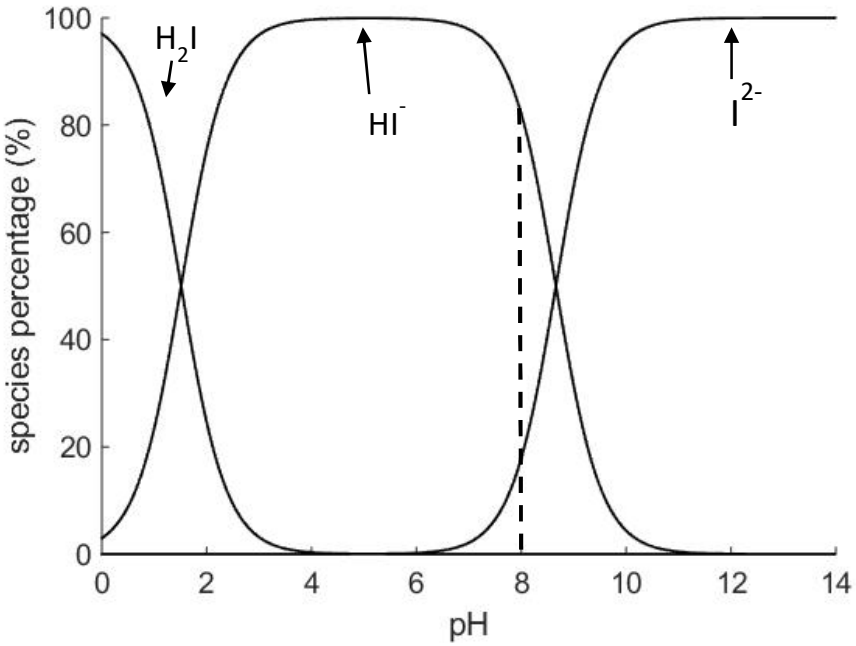

Figure 2. Bjerrum plot showing the species distribution of purified mCP as a function of pH (T = 298.15K, S = 0). The mCP indicator solution is usually adjusted to pH = 8.0 (the dash line), where HI^- = 80%, and I^{2-} = 20%.

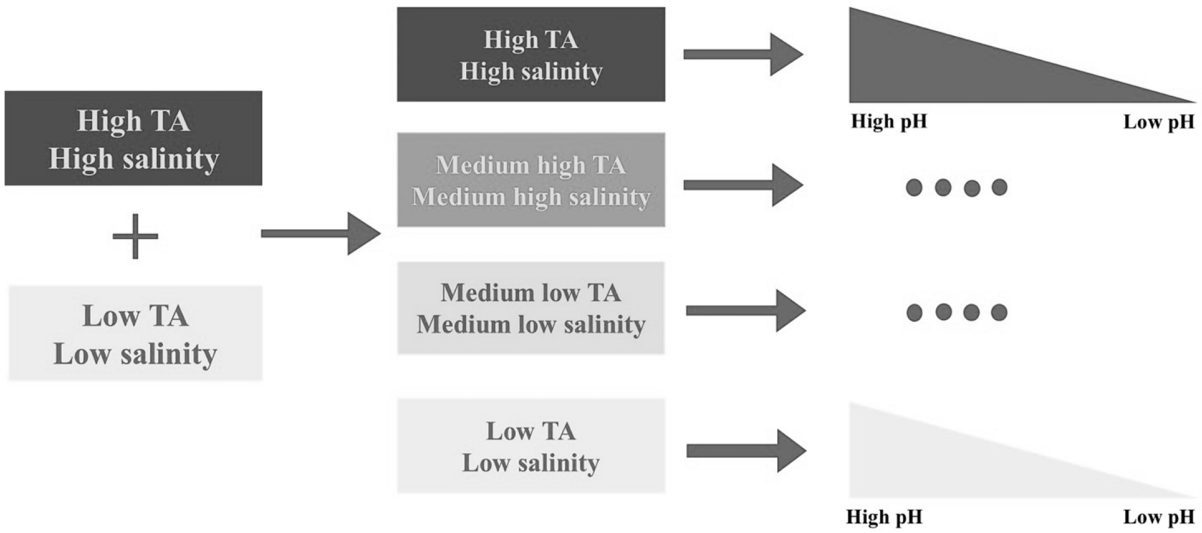

Figure 3. The laboratory experiment design of fixed S and TA relationship. High TA-S water mixed with low TA –S water to get 4 types of water with different TA and salinity. Each type of water was adjusted to obtain a pH gradient by dissolving/removing CO_2.

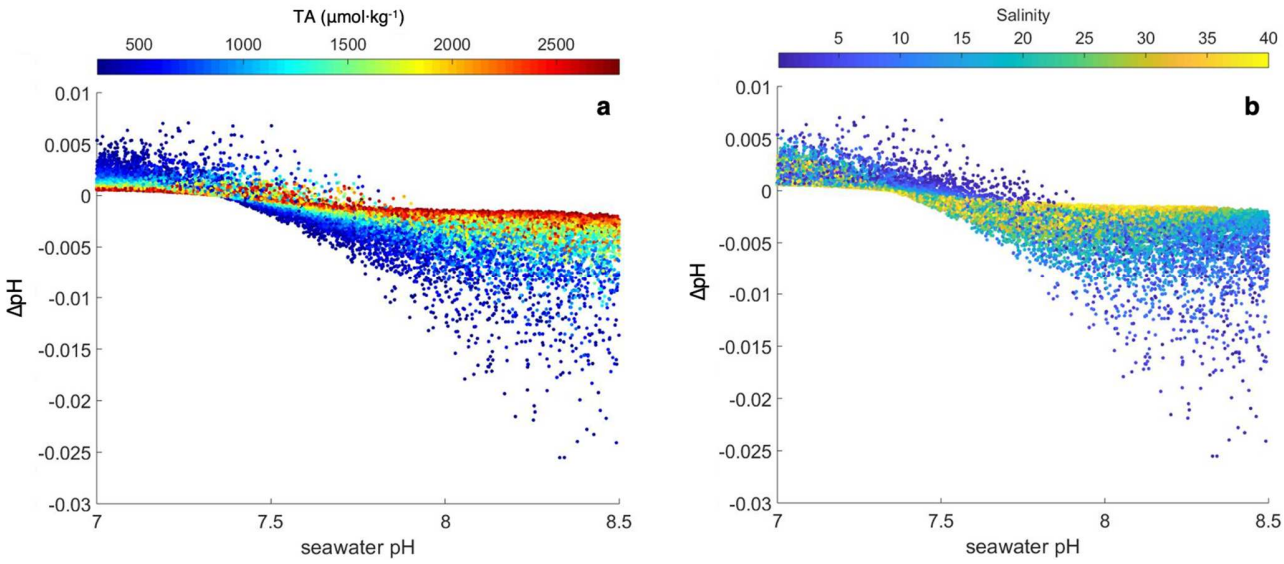

Figure 4. Dye perturbation simulation on sample pH using 50000 random combinations of DIC, TA, and S with a dye stock of S = 0 and pH = 8. The change in pH caused by the dye addition is shown on the Y axis as ΔpH (seawater pH with dye addition – seawater pH) as a function of sample pH in absence of the dye (X axis). Figure 3a visualizes the variation in ΔpH with TA while 3b shows the variation in ΔpH with S. Both panels indicate the influence of TA and salinity on dye perturbation.

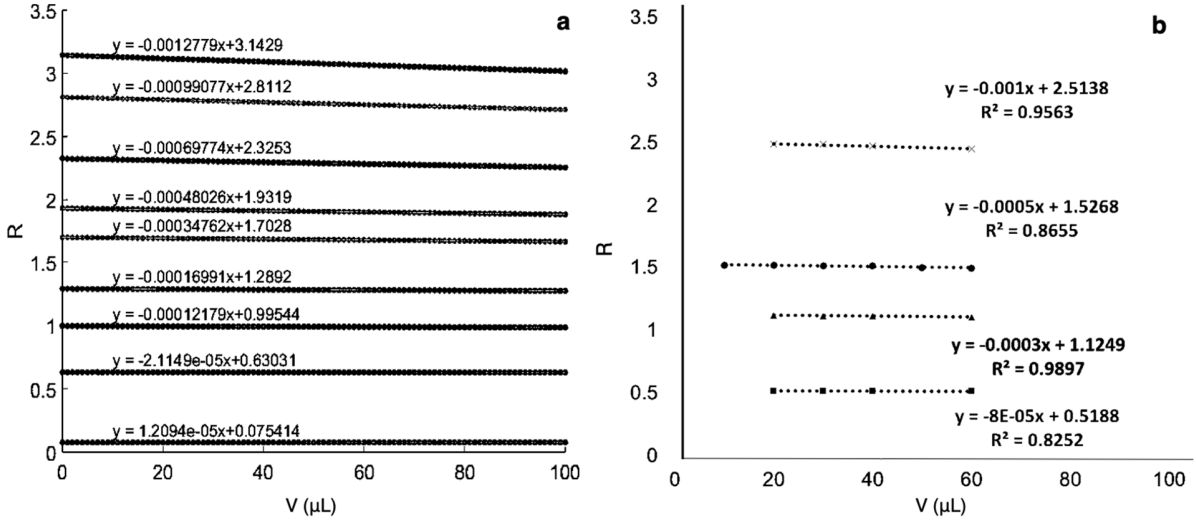

Figure 5. The absorbance ratio (R) as a linear function of dye volume (V). Supplot (a) is simulation result. Each line represents a different combination of sample DIC, TA and S, thus a different pH. Subplot (b) is laboratory result, supporting the simulation results.

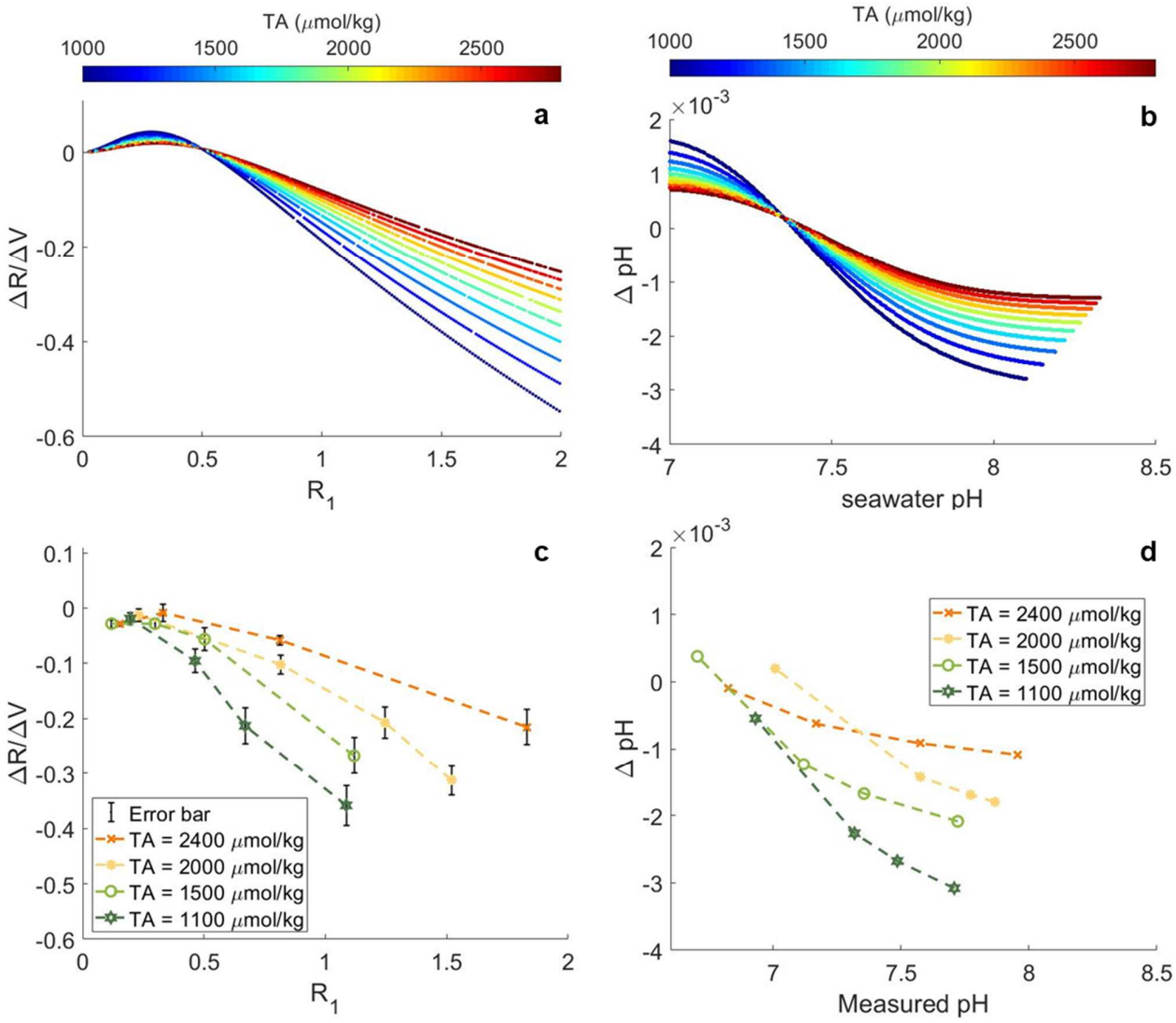

Figure 6. Simulation (a and b) and experimental (c and d) results of dye perturbation on a sample with fixed high salinity (S = 36) and variable TA. The high S-TA is Gulf of Mexico Seawater, while the high S – low TA water is the Gulf of Mexico Seawater with HCl addition. Subplots a and c show the relationship between $\Delta R/\Delta V$ and R_1, which depends on the sample TA. Subplots b and d show the ΔpH (= pH with dye perturbation – pH without dye perturbation) changes of the water sample due to the indicator addition.

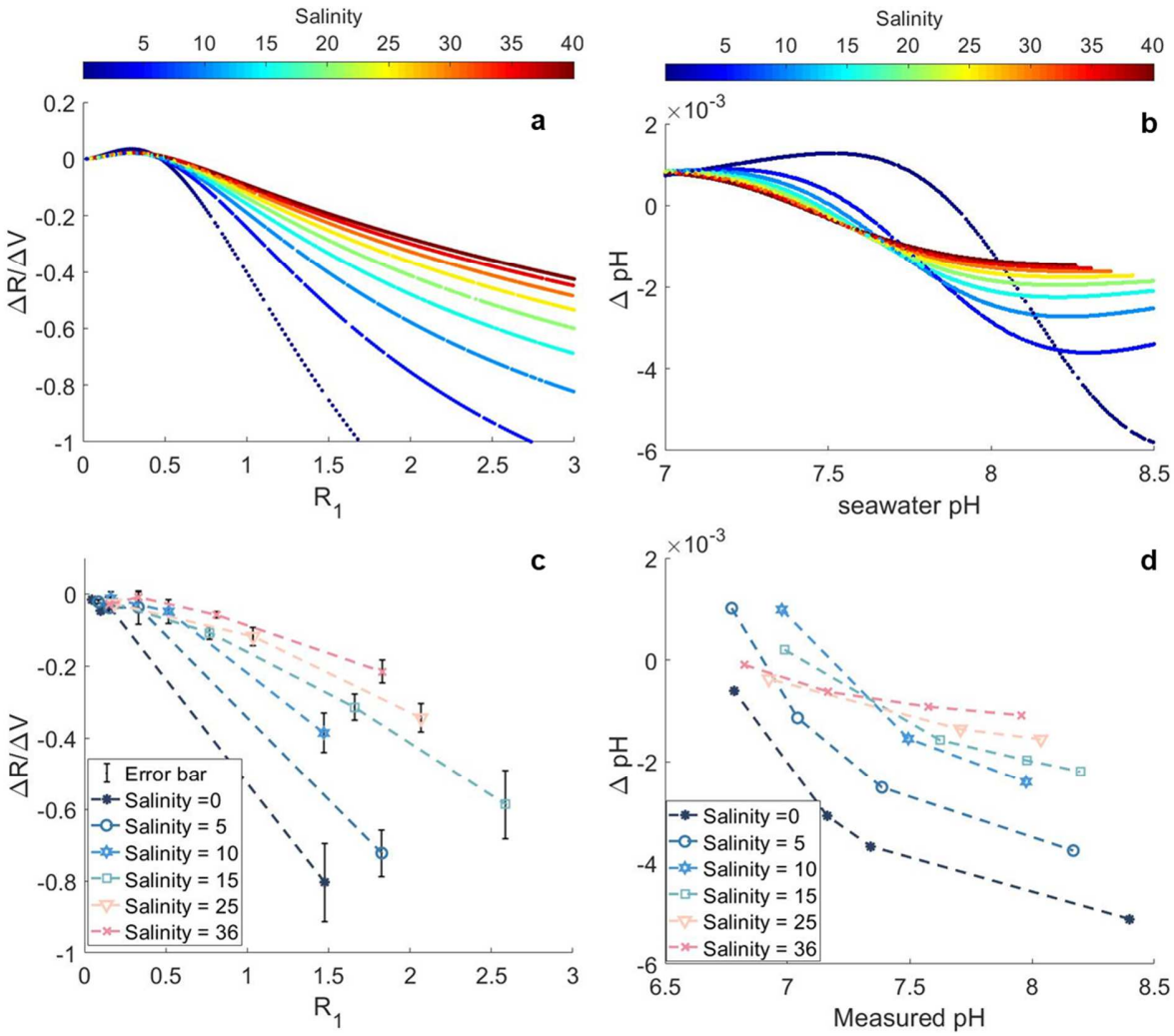

Figure 7. Simulation (a and b) and experimental (c and d) results of dye perturbation on the sample with fixed high TA (TA = 2350 μmol kg^{-1}) and variable S. The high S-TA is Gulf of Mexico seawater, while the low S – high TA is from Mississippi river water. Subplots a and c show that the decreasing rate of $\Delta R/\Delta R \sim R_1$ depends on the sample S. Subplots b and d represent the ΔpH (= pH with dye perturbation – pH without dye perturbation) changes of the water sample due to the indicator addition.

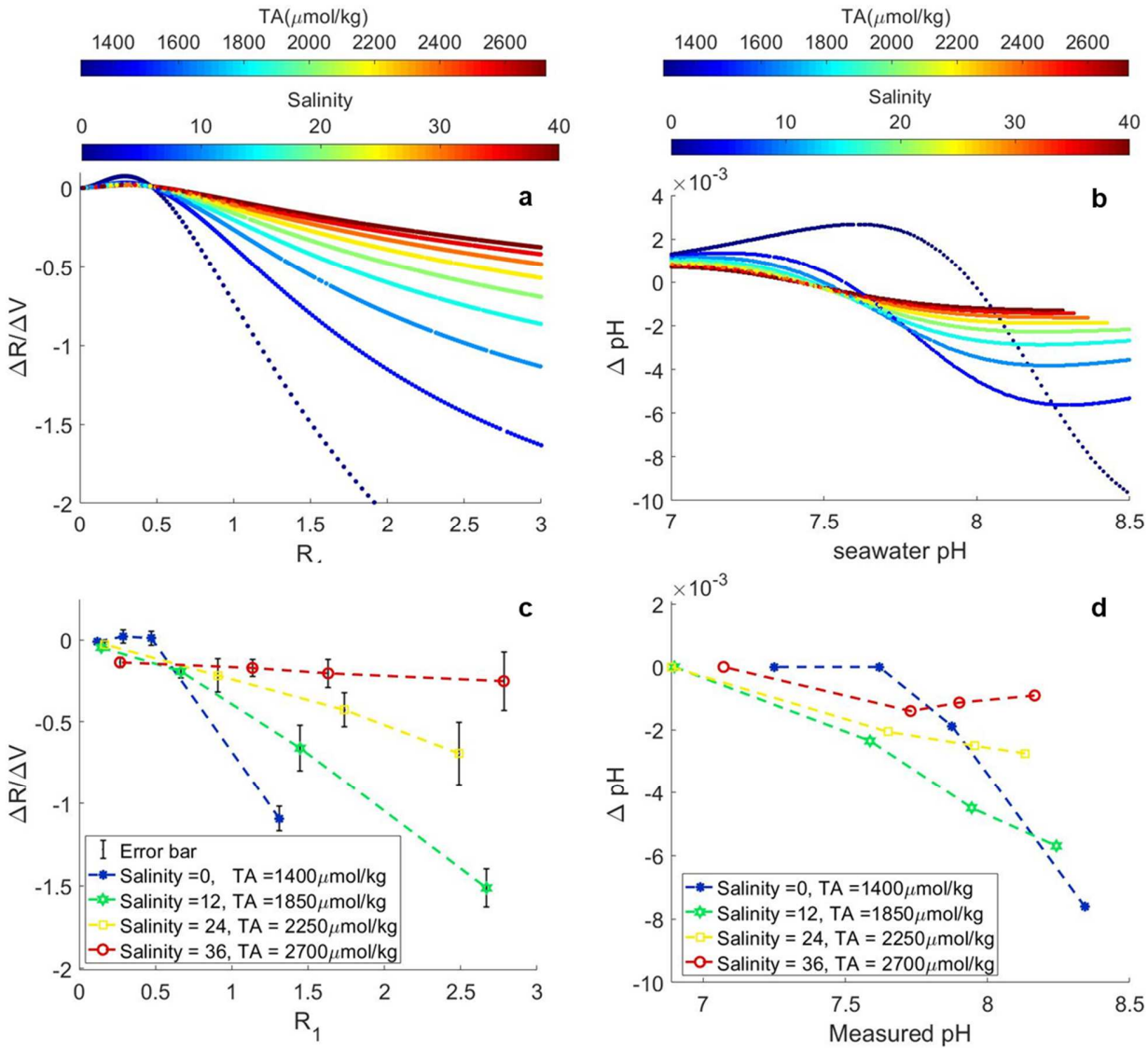

Figure 8. Simulation (a and b) and experimental results (c and d) of dye perturbation on the sample with fixed TA –S relationship. The high S-TA is Gulf of Mexico Seawater, while the low S – low TA is the Atchafalaya river water with HCl addition. Panels a and c shows that the decreasing rate of ΔR/ΔV and R_1 decrease with TA and salinity increasing. Panels b and d shows the effect of dye perturbation on pH is smaller for high TA and salinity samples.

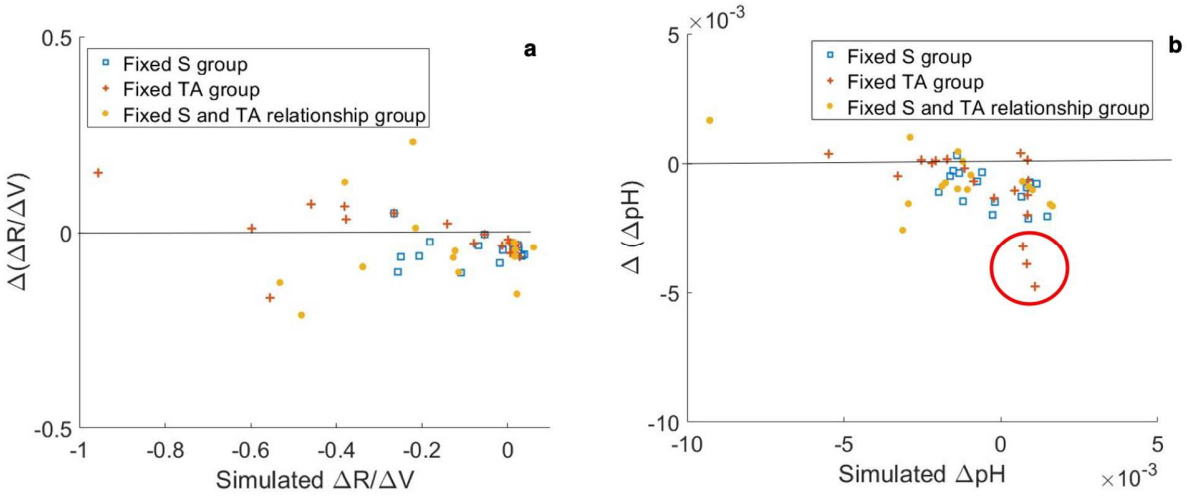

Figure 9. Comparison of simulated vs. experimental ΔR/ΔV (a) and ΔpH (b). Y axis is the difference between experimental value and simulated value. Outliers in the red circle are the low salinity samples with fixed high TA. Δ(ΔpH) and its related uncertainties are limited by the accuracy and precision of spectrophotometric pH measurement and the carbonate chemical constants at low salinity (S<5).

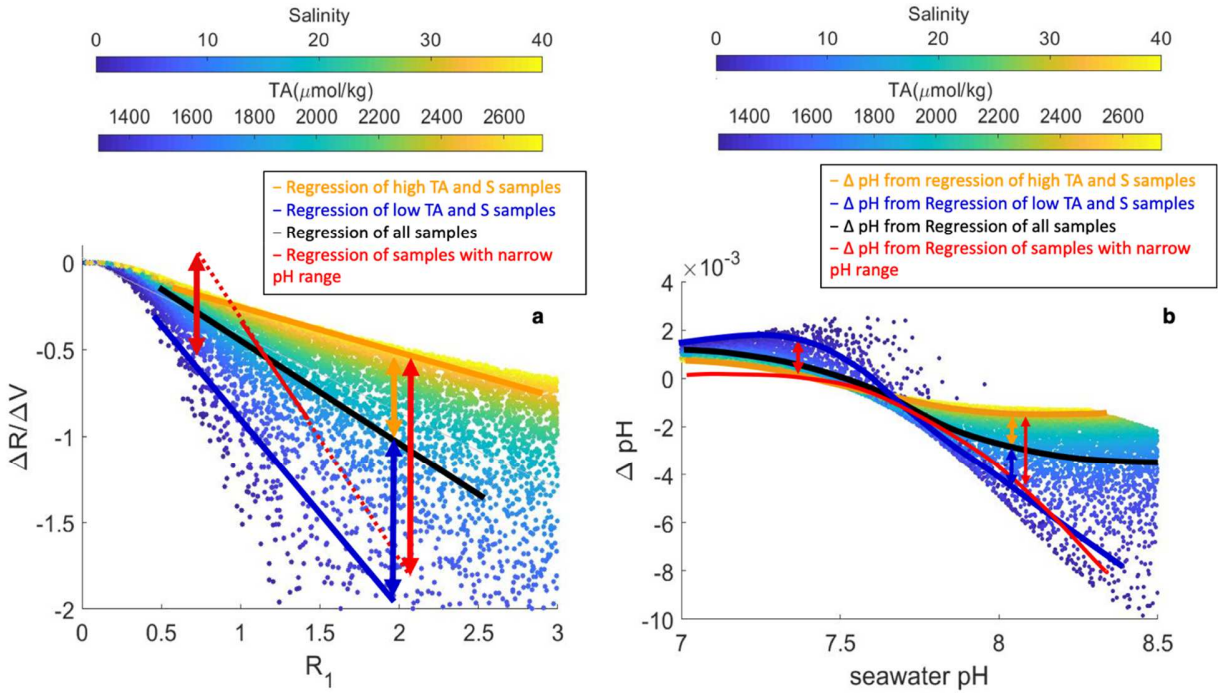

Figure 10. Possible pH biases caused by the empirical dye perturbation. Subplot a represents the distribution of ΔR/ ΔV versus R_1. Subplot b shows the dye perturbation on pH (ΔpH). Black and red arrows indicate the differences of regression lines (subplot a) and the differences of ΔpH (subplot b).

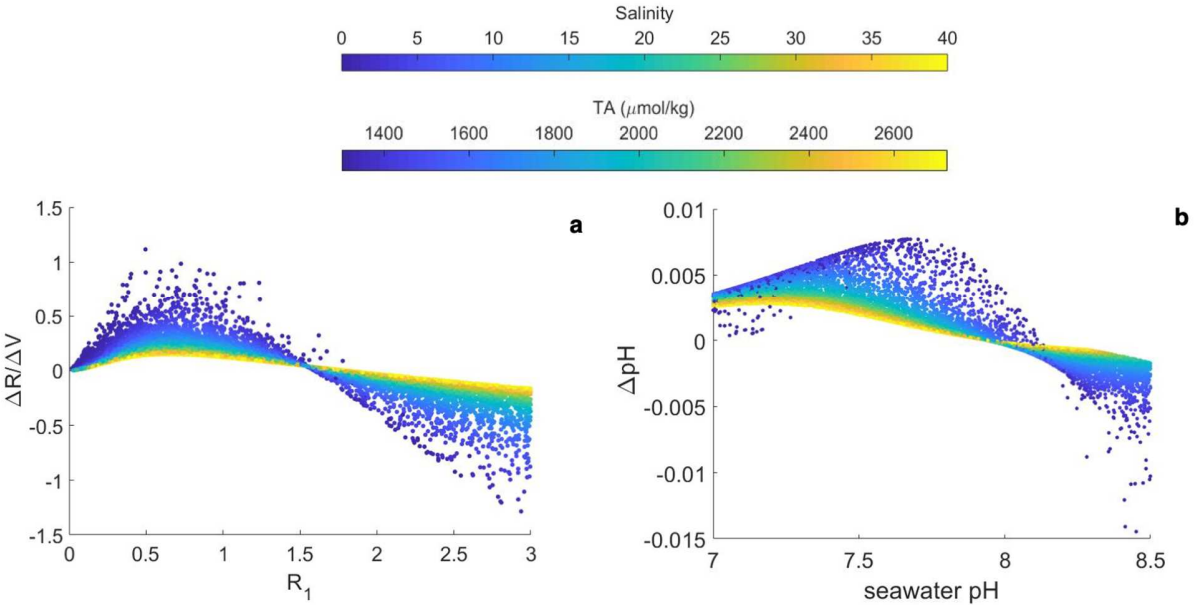

Figure 11. The dye perturbation on sample pH with dye S = 35, dye pH =8.0. The influence of the dye perturbation is smaller for high S-TA water than for low S-TA water. Subplot a shows $\Delta R/\Delta V$ vs R_1. $\Delta R/\Delta V$ vs. R_1 has a linear relationship when $R_1 > 0.5$. Subplot b shows that when sample salinity and pH are close to the dye, ΔpH is close to 0.

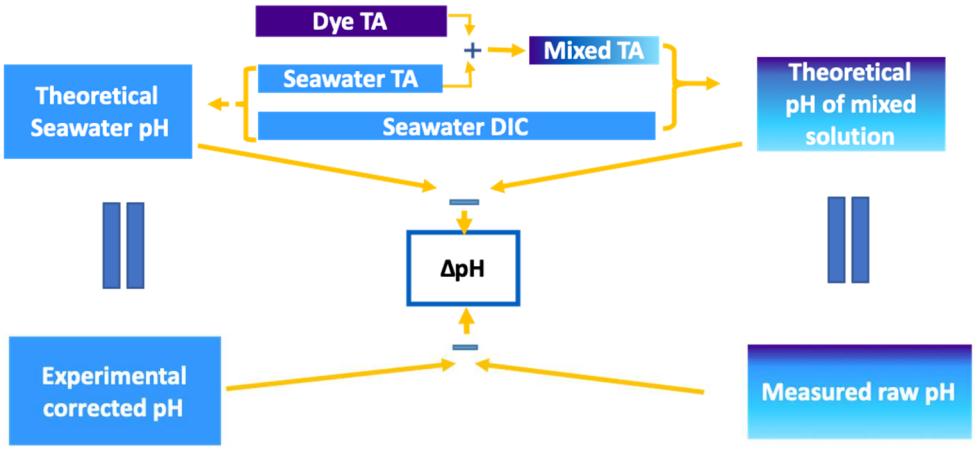
Dye TA
Mixed TA
Seawater TA
Seawater DIC
Theoretical Seawater pH
Theoretical pH of mixed solution
ΔpH
Experimental corrected pH
Measured raw pH

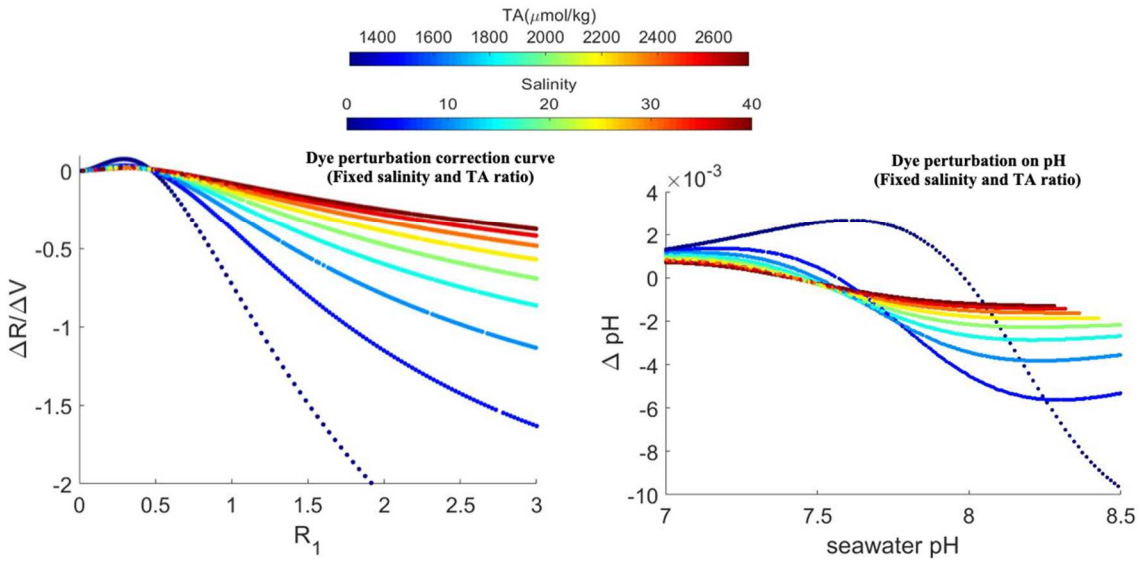
TA(μmol/kg)
1400 1600 1800 2000 2200 2400 2600
Salinity
0 10 20 30 40
Dye perturbation correction curve
(Fixed salinity and TA ratio)
ΔR/ΔV
R1
Dye perturbation on pH
(Fixed salinity and TA ratio)
×10-3
Δ pH
seawater pH